Ultra short-time dynamics of radiation damage in fcc metals

Marc Hayoun,* Gerrit Coddens, and Guillaume Petite
Laboratoire des Solides Irradiés, Ecole Polytechnique, CEA-DSM-IRAMIS, CNRS, 91128 Palaiseau, France
(Received 12 May 2009; revised manuscript received 31 July 2009; published 11 November 2009)

We have performed molecular-dynamics simulations of displacement cascades in copper in order to investigate the nonequilibrium ultra-short-time damage and to evaluate the possibility of observing it experimentally *in situ* (e.g., in a pump/probe laser experiment). The atomic trajectories have been analyzed by calculating their x-ray diffraction patterns as a function of time. The results show that an integrated x-ray intensity can indeed be used to evidence the irradiation effects. Even though the number of Frenkel defects is large, the main effect of the irradiation showing up in the x-ray intensities at ultrashort times is an important alteration of the lattice vibrations. On the basis of these results, a pump/probe setup is proposed.

DOI: 10.1103/PhysRevB.80.184204 PACS number(s): 61.82.Bg, 02.70.Ns, 61.05.cp, 61.72.J−

I. INTRODUCTION

Present-day laser equipment permits to obtain very short and intense laser pulses, which can be used to produce many kinds of short and intense bursts of secondary particles with a broad spectrum of energies. These secondary particles can be, e.g., neutrons, electrons, protons, or x-rays. Ultrashort x-ray pulses are usually produced in the interaction of an intense visible ultrashort laser pulse with a hot and dense plasma, using either solid or gaseous targets. Depending primarily on the target atomic number, the x-ray spectrum can consist of sharp spectral lines (e.g., K_α radiation of light elements[1]), broader unresolved transition arrays or even continuous Brehmsstrahlung radiation.[2] In the most recent experiments, where the laser-plasma interaction occurs in the relativistic regime, synchrotron radiation of the laser-driven electrons can produce high-intensity broadband emission in the 1–10 keV photon energy range, the so-called "betatron radiation."[3] Likewise, in this relativistic regime, femtosecond pulses of high-energy electrons and protons (the latter with energies up to tens of MeV) can be obtained.[4,5] Their energy spectrum is usually continuous, though the latest developments using reduced-mass targets show that also monochromatic particle beams can be obtained. A specific feature of all such laser-driven pulsed particle sources is that the high-energy radiation emission is precisely timed with the driving laser pulse, opening the possibility of "pump-probe" experiments using such sources.

When a high-energy proton impinges onto a solid target it produces a displacement cascade. Many molecular-dynamics (MD) simulations have been performed to study the physics of such displacement cascades in various solids,[6–8] but on certain issues the confrontation between theory and experiment has remained rather indirect. In fact, the simulations show that at short times a displacement cascade produces a large number of Frenkel defects,[6,8,9] but these large numbers have never been observed experimentally, as the vast majority of these defects only exist for fleeting moments. They recombine very quickly, e.g., within 10 ps, such that only a tiny fraction of the initially created pairs survive this self-annealing process by the time one tries to observe them with different equipment. Similarly, the surplus energy the impinging particle puts into the sample, creating the cascade, which is characterized by a set of larger instantaneous local values for $\langle u^2 \rangle$ over a limited spatial extent, gradually diffuses away with time. To have a chance to observe displacement cascades and their Frenkel defects one must therefore find a way to probe a cascade *in situ*. Ultrashort laser pulses in a pump/probe setup provide exactly the combination of experimental facilities needed to observe the cascades. The idea is thus to produce both a pulsed proton beam and a pulsed x-ray beam from two derivations of the femtosecond-pulsed laser beam. Let us assume that we are able to produce a pulsed proton beam of more or less well-defined energy. We assume also that we are able to determine exactly at which time t_0 each pulse will reach the solid target. By varying the path length of the laser beam derivation that produces the x-ray pulses one can then choose the delay time t corresponding to the moment in time t_0+t at which we probe the cascade. Hence, we could probe the time evolution of the cascade and the Frenkel effects over the whole time span during which they pop in and out of existence.

The present paper reports on a MD simulation of such a difficult type of experiment. The work has thus really to be situated within the context of the emerging experimental possibilities mentioned above, rather than within a context of deriving results about displacement cascades (for which the existing literature is already very complete). We simulate displacement cascades in a copper single crystal as produced by the impact of a proton with a kinetic energy K_p of 49.2 keV. This value corresponds to a kinetic energy K_{Cu} of 3 eV for the recoiling copper atom in a head-on proton collision, as calculated from the relation:[10]

$$K_{\mathrm{Cu}} = 4K_p \frac{M_p M_{\mathrm{Cu}}}{(M_p + M_{\mathrm{Cu}})^2} \cos^2 \psi, \tag{1}$$

where the angle $\psi=0$ in a head-on collision; M_p and M_{Cu} are the masses of the incident and target particles, respectively. Multiple recoils within a single cascade, corresponding to the impinging proton hitting two atoms in the lattice in succession have not been considered. Also possible interactions between two displacement cascades that could be produced more or less simultaneously in an extremely high proton-flux have not been considered. The momentum of the proton has been assumed to be along the y direction, which corresponds

to the (010) direction of the copper single crystal. Simultaneously, we have calculated the x-ray diffraction diagram of the simulation box at different times t_0+t after the simulated proton impact at time t_0. Hence, we have monitored the time evolution of this diffraction diagram while the cascade develops. This combination of direct-space and reciprocal-space data should in principle allow us to learn how the diffraction spectra have to be interpreted. We anticipate that this could be a valuable aid for experimental-protocol design, and give added value to the experimental data. In order to avoid confusion, it should be noted that the time dependence of the elastic intensity is not a dynamical signal. In order to obtain a dynamical signal, one must correlate the Fourier amplitudes at two different times.

II. SIMULATION AND ANALYSIS OF THE ATOMIC TRAJECTORIES

A. Molecular dynamics

The MD (Refs. 6–8, 11, and 12) computations have been performed in the microcanonical ensemble. The modeling of the copper interactions relies on an empirical n-body potential of the tight-binding type that reproduces satisfactorily its physical properties.[13–15] The simulated system is a cubic box of size L^3 ($L=14$) containing 10 976 copper atoms. Periodic boundary conditions (PBC) are employed and the time step is equal to 5×10^{-16} s. We did not introduce any damping of the motion of the boundary atoms.[16] In fact, we did not want that the tool used to regulate the number of artifacts that might occur in our simulations (due to the PBC), could introduce itself some additional perturbation. We therefore have limited our means of control to varying the box size. Kinetic disturbances may, thus re-enter the MD box unless its size is large enough and the temperature rises due to the kinetic energy dissipated by the primary knock-on atom (PKA). In order to avoid finite-size effects in the calculations of the x-ray intensities, we have considered the MD box as embedded into a large perfect cubic geometrical crystal (see Sec. II B).

Twenty-one independent equilibrium configurations of the copper crystal (decorrelated by a time evolution of 10 ps) have been generated at a temperature of 302 K and a pressure close to zero for a lattice parameter of 3.6358 Å. The zero of the time scale of the 21 ensuing irradiation simulations corresponds to these equilibrium configurations. The displacement cascades are initiated at $t=0.005$ ps by the transfer of kinetic energy to a single copper atom. This simulates a recoil. We have not introduced statistical distributions for the initial recoil parameters of the PKA. In all 21 simulation runs the momentum transfer has always been aligned along the (010) direction of the FCC lattice and the kinetic energy transfer has always been given the same constant value. This unusual choice of initial conditions[6] permits to reduce the complexity of the analysis of the x-ray diffraction patterns by only studying the (010) direction. This is justified in a preliminary study wherein the only aim is to explore the experimental possibilities to observe the ultra-short-time damage *in situ*. The statistical distribution of the PKA recoil parameters will be taken into account in a future work including the experiment.

As the number of atoms in the simulation box is small there is a complete loss of any structure in the system if the knock-on energy is taken too large. The energy transferred to the copper atom in our simulations has therefore been fixed at the value of 3 keV in order to avoid such problems.

B. X-ray intensity calculations

The x-ray intensities in the present paper are expressed in physical units. This means that the wave vector $\boldsymbol{q}$ is expressed by the formula $q=2\pi/\lambda$, as opposed to the expression $q=1/\lambda$ often used in crystallography, where traditionally units 2π are being used. Here, 2θ is the scattering angle, and λ the wavelength of the x rays. We note the transfer of wave vector occurring in the scattering process as $\boldsymbol{Q}=\boldsymbol{q}_{\text{out}}-\boldsymbol{q}_{\text{in}}$. We have adopted a special approach for the calculation of the x-ray intensities I. It is well known that they are given by $I=|\mathcal{F}(\boldsymbol{Q})|^2$, where $\mathcal{F}(\boldsymbol{Q})$ is the Fourier amplitude. The approach permits to avoid truncation problems and to obtain results that are rigorously exact.

For the calculation of the Fourier amplitude $\mathcal{F}(\boldsymbol{Q})$ of a one-dimensional periodic lattice of N atoms along e.g., the x-axis, we restrict ourselves to a set S of $\boldsymbol{Q}$ values $Q=2\pi k/Na$, where a is the lattice parameter and k is an integer. The crystal lattice points are situated in $x_j=ja$, where j is an integer. We obtain then in a straightforward manner,[17]

$$\mathcal{F}(Q)=\sum_{j=1}^{N} e^{iQx_j}=N\sum_{n}\delta(Q-Q_B), \tag{2}$$

where $Q_B=n(2\pi/a)$ and n runs over Z. This means that there is a reciprocal lattice of Bragg peaks with weight N in Q_B. For the remaining Q values in the set S, the Fourier amplitude $\mathcal{F}(Q)$ is zero, exactly as would be the case in an infinite perfect crystal in all points of reciprocal space that do not correspond to the location of a Bragg peak. But for the Q values that do not belong to the restricted set S of multiples of $2\pi/Na$, the algebra no longer reproduces the correct zero result that would apply for an infinite perfect crystal. This is hardly surprising, as we have not calculated the Fourier transform of an infinite crystal. In fact, the algebra is exact for a finite crystal. Our problem is rather that we want to remove the finite-size effects from our calculations. The algebra shows that we can achieve this by making our calculations on the set S. This result is easily generalized to three dimensions.

This calculation illustrates why fast Fourier transform (FFT) programs cannot be used without observing a number of caveats. They can, e.g., give wrong answers for the diffraction spectrum of a periodic lattice if the period of the FFT is not adapted to the lattice period of the crystal, such that the points where the Fourier transform is calculated are not on the set S. The FFT is then subject to finite-size truncation problems. One must therefore be careful about interpreting the significance of tails in Bragg peaks in a spectrum obtained from a FFT. Also a number of numerical values for the dimensions of the simulation box have to be excluded in

order to avoid malfunctioning of the FFT. Given the rather small dimensions of our simulation boxes this would have been a severe limitation.

We have therefore adopted the different approach described above. We consider the cubic simulation box B of size L^3 as embedded into a large, perfect cubic geometrical crystalline lattice G of size D^3. That is, we mentally cut a cubic hole H of dimensions L^3 into the geometrical crystal with exactly the same size L^3 as the simulation box, and again mentally, enter the simulation box into this hole. This has to be done carefully such that one does not introduce any discontinuity in the average interatomic distances across the boundaries between G/H and B. For example, in order to avoid lattice parameter mismatch problems that could be induced by the variation in the lattice parameter with temperature, the simulations have been carried out at constant volume. The Fourier transform to be calculated is then obtained as $\mathcal{F}[G]-\mathcal{F}[H]+\mathcal{F}[B]$. Both $\mathcal{F}[G]$ and $\mathcal{F}[H]$ can be calculated analytically, and the rigorous result can be coded directly into the program. The ensuing results are exact: for example, the Bragg peaks contained in the Fourier transform $\mathcal{F}[G]$, and calculated according to Eq. (2), are pure Dirac measures without any tails. The simulation box B is sufficiently small to allow for a calculation of its Fourier transform $\mathcal{F}[B]$ that is purely based on its definition. Hence we avoid this way the truncation effects inherent to the FFT mentioned above. Actually, we perform these calculations on the atomic positions. A real crystal is the convolution of its set of atomic positions $(G\backslash H)\cup B$ with an atomic decoration. In our case this atomic decoration consists of copper atoms. In the Fourier transform, this means that we must multiply the Fourier transform of this set with the atomic form factor of the copper atom. The calculation of this atomic form factor has been performed using the method and the tabular values given in reference.[18] By varying the size D^3 of the large crystal, we can actually simulate the volume fraction of the crystal that is irradiated in the real experiment. We may note that the copper lattice is not a Bravais lattice and that this leads to extinction rules for some Bragg peaks, which we have calculated. In fact, the FCC unit cell contains four copper atoms and the lattice parameter that has been used is 3.6358 Å.

One effect of using PBC is rather important for the calculations of the Fourier transform. The energy and momentum we confer to the PKA are conserved quantities. Eventually they become redistributed over all the atoms of the simulation box. This results in a uniform motion in the y-direction of the center of mass of the simulated lattice. As the energy conferred to this single atom is large on the scale of the lattice dynamics and as the number of atoms in the simulation box is rather limited, this effect becomes readily observable. One by one the lattice planes reach the "upper" boundary of the box in the y direction. There they "jump"—from the viewpoint of the calculation of the Fourier transform to the "lower" boundary in the y direction, due to the PBC. The phase factor in the Fourier transform that corresponds to this translational jump interferes with the phase factor of the Fourier transform of the perfect crystal by the time we square the Fourier amplitudes in order to obtain the x-ray intensities. This introduces a severe error into the calculated intensities under the form of oscillations in the time dependence, which does not correspond to any physical reality. This uniform center-of-mass motion has therefore been corrected for in the analysis of the computed data.

C. Integration of x-ray intensities

Since the intensities are weak we have integrated them along the line at $q_z=0.2$ Å^{-1} and $q_x=0$ Å^{-1}. The choice of q_z permits to avoid that the strong intensity of the Bragg peaks outweighs the intensities of the small signal we are interested in. The intensities are stored as a function of q_y for each selected time of the MD trajectory. The integration is then performed along the q_y axis.

D. Frenkel defects

An atomic site is defined by considering a spherical volume centered on a geometrical regular lattice site. The value of the radius of the sphere is chosen in such a way that a moving atom leaving a regular site is discriminated from a vibrating atom with a large magnitude at the equilibrium temperature. When this volume is empty there is a vacancy on the site. If an atom does not belong to any atomic site it is an interstitial atom. Such a pair of an interstitial atom and a vacancy defines a Frenkel defect. The actual value of the radius of the sphere in the simulations was 0.84 Å. This value can be compared to the vibration amplitude $\langle u^2\rangle^{1/2}=0.118$ Å at the equilibrium temperature finally reached by the irradiated system, which is 600 K. We have developed a code, based on this definition of the Frenkel defects, to count them in direct space along the MD trajectories.

E. Further analysis

The code permits to remove *a posteriori* the Frenkel defects from a given configuration by putting the interstitials on an empty lattice site. The off-Bragg Fourier intensity of the resulting manipulated configuration yields the contribution of the phonons to the x-ray signal. The same code permits also to "kill" *a posteriori* the phonon dynamics of all on-site atoms in a configuration by putting them on the geometrical lattice position of the site they are "on" in the configuration. The off-Bragg Fourier intensity of the resulting manipulated configuration yields the contribution of the Frenkel defects to the x-ray signal.

III. RESULTS AND DISCUSSION

A. X-ray intensities

Figure 1(a) shows the x-ray diffraction intensities in the $q_z=0$ plane obtained from the MD simulation of the 600 K nonirradiated system. The Bragg peaks can be clearly distinguished. Their intensities are modulated by the Debye-Waller factor. On this intensity scale the thermal diffuse scattering due to phonons or lattice defects is not visible. Therefore, we show on Fig. 1(b) the intensities from the same simulation in the nearby reciprocal lattice plane $q_z=0.2$ Å^{-1} where the absence of Bragg peaks permits to visualize the lattice vibrations on a full scale.

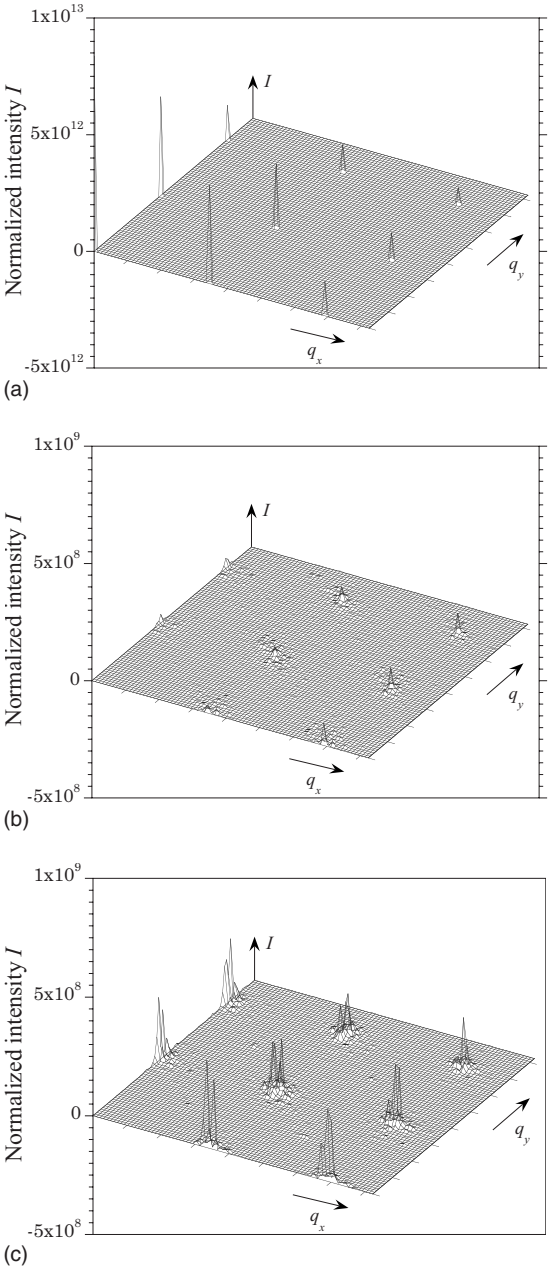

FIG. 1. Three-dimensional reciprocal-space plots of the normalized calculated x-ray intensity I vs (q_x, q_y) for three nonaveraged single-history runs. Each tick on the q_x and q_y axes corresponds to 1 Å^{-1}. The temperature of the nonirradiated system was chosen close to the final equilibrium temperature of the irradiated system for comparison. (a) Bragg peaks in the plane $q_z=0$ Å^{-1} for the nonirradiated system at 600 K. (b) Intensities in the off-Bragg plane $q_z=0.2$ Å^{-1} for the same nonirradiated system at 600 K. (c) Intensities in the same off-Bragg plane $q_z=0.2$ Å^{-1} for the irradiated system at 300 K after a relaxation time of 0.60 ps.

These data can be directly compared with those of Fig. 1(c). Fig. 1(c) displays the x-ray diffraction intensities in the same reciprocal lattice plane $q_z=0.2$ Å^{-1} from a snapshot at 0.60 ps after knock-on in the MD simulation of the 300 K irradiated system. We must stress that the time scale of 0.60 ps selected here is much shorter than in traditional simulations. The intensity scales of Figs. 1(b) and 1(c) are identical.

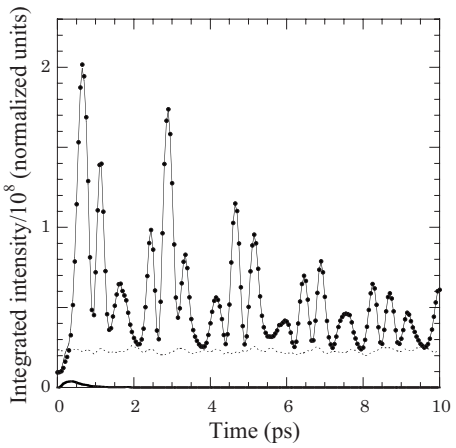

FIG. 2. Time evolution of the integrated x-ray intensities (averaged over 21 independent runs) for the system irradiated at 300 K (full line) and for the nonirradiated system at 600 K (dotted line). The temperature of the nonirradiated system was chosen close to the final equilibrium temperature of the irradiated system for comparison. A decomposition of the integrated intensities of the irradiated system into two components is also shown: the thick line corresponds to the contribution from the off-site atoms which give rise to the Frenkel defects whereas the full circles represent the complementary intensity from the on-site atoms.

From the comparison it is obvious that there is additional diffuse scattering intensity in the irradiated system.

This significant extra intensity is the x-ray diffraction fingerprint of irradiation effects in a metal and as such could be used to monitor them. However, in a real experiment the lattice vibrations from the nonirradiated part of the crystal will be superimposed on them. In order to increase the statistics, we have integrated the signal in this plane with respect to q_y along the line $q_x=0$. All the results presented hereafter will refer to this particular type of integrated intensities.

B. Integrated x-ray intensities

The result from these integrations as a function of the simulation time is reported in Fig. 2. As mentioned above, the zero of the time scale corresponds to an equilibrium configuration while the knock-on takes place at $t=0.005$ ps. All the data are averages over 21 independent simulation runs. The equilibrium temperature eventually reached by the irradiated system is close to 600 K. We have therefore also performed 21 equilibrium MD simulations on a nonirradiated system for comparison. The associated integrated x-ray intensities are also reported in Fig. 2.

It is obvious that the time dependence of the intensity in the nonirradiated system is featureless and that the intensities are much lower than those of the oscillating signal from the irradiated system. Hence, this oscillating time dependence is characteristic of an irradiated sample.

C. Rôle of the Frenkel defects

In order to understand the origin of this large oscillating signal we have identified the positions of all vacancies and

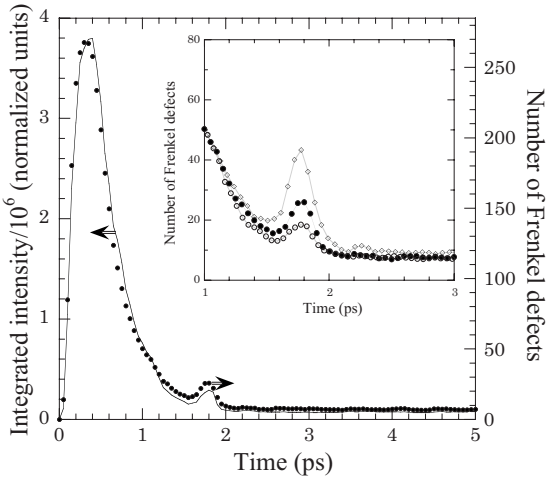

FIG. 3. In the main plot we compare the number of Frenkel defects (full circles) obtained from direct-space counting with the integrated x-ray intensities from the off-site atoms (full line). The latter is the same signal as shown in Fig. 1 but now on an appropriate scale. The arrows identify the scale for each quantity. Both quantities are averages obtained from 21 independent runs. The small second peak at 1.8 ps is an artifact of the PBC. The insert gives the evidence for this. It displays the number of Frenkel defects in this peak for the three different sizes of the MD box used. The time has been rescaled by the linear dimension of the MD box as discussed in the text. The full circles correspond to the 10 976-atom cell as in the main plot, the diamonds to the 8 788-atom cell and the open circles to the 13 500-atom cell.

interstitials (the off-site atoms), i.e., of all Frenkel pairs. After this, we have repositioned artificially in each configuration all other atoms on geometrical lattice sites. This enabled us to calculate the contribution of the Frenkel defects to the oscillating signal. This contribution is also displayed in Fig. 2 and it can be seen to be very small. Only up to 1 ps does it represent some observable intensity. The contribution from the on-site atoms was obtained alternatively by repositioning artificially all off-site atoms on the open lattice sites. It coincides almost perfectly with the total integrated x-ray intensity. In summary, we (i) conclude that the contribution of the Frenkel defects can be ignored, and (ii) we attribute the oscillating signal therefore in terms of lattice vibrations that have been altered by the developing cascade.

Figure 3 validates further the analysis of the contribution from the Frenkel defects. It compares the x-ray intensity due to the Frenkel defects discussed above with the number of these defects obtained by direct counting along the MD trajectory. In fact, both quantities display exactly the same time dependence. The small second peak at 1.8 ps is an artifact of the PBC, as will be discussed in Sec. III E.

D. Long-time scale

Figure 4 displays the behavior of the time dependence of the integrated x-ray intensities on a much longer time scale and with a coarser time step than in Fig. 2, for two single MD runs. Up to 15 ps the signal from the irradiated sample is significantly larger than the signal from the 600 K nonirradiated system. On the long-time scale however, the intensities of the two signals become comparable, in agreement with our statement that the equilibrium temperature reached by the irradiated system is approximately 600 K.

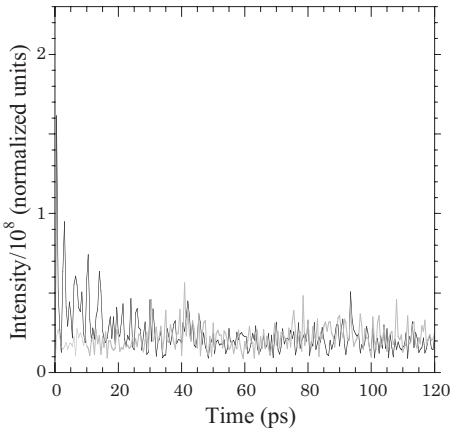

FIG. 4. Evolution of the integrated x-ray intensities on a long-time scale of single runs for the system irradiated at 300 K (full line) and for the nonirradiated system at 600 K (gray line). As (i) the curve does not represent an average over independent runs and as (ii) its portion between 0 and 10 ps has been drawn with a poorer time resolution than in Fig. 1, the visible intensity variations are not identical to those observed in Fig. 1. One observes that the irradiated system has reached equilibrium after 30 ps and that this equilibrium state is characterized by intensity fluctuations similar to those of the nonirradiated system at 600 K. Hence, the short-time signal is truly characteristic of the irradiation.

E. Size effects

We remind the reader that we have made sure that there are no finite-size effects in the calculation of the Fourier transforms (see Sec. II B).

In order to estimate the importance of finite-size effects in our MD simulations, we have performed calculations for two additional sizes of the simulations box, viz., one with 8788 ($L=13$) and one with 13 500 atoms ($L=15$). In Fig. 5 we show the same signal as in Fig. 2 for the three box sizes. The signal is clearly size dependent.

In Fig. 6 we show the same results after a renormalization of the time scales with the linear dimension of the simulation box. On this effective time scale the size dependence no longer shows up. We interpret this result as evidence that the x-ray intensities result mainly from acoustic phonons. This also means that the size effects in our MD simulations are well understood and that they do not bias our conclusions.

The dispersion curves for the acoustic phonons of a $N \times N \times N$ periodic lattice with periodic boundary conditions are not continuous lines, but rather consist of $N \times N \times N$ discrete wave vectors with their corresponding frequencies.[17] In the long-wavelength limit, the dispersion relation is linear ($\omega = vq$, where v is the speed of sound), such that the frequencies scale with $1/N$. It is therefore possible to renormalize the time dependences for the various box sizes with N.

Another size effect is illustrated in Fig. 3. The small second peak at 1.8 ps is an artifact due to the PBC. This is

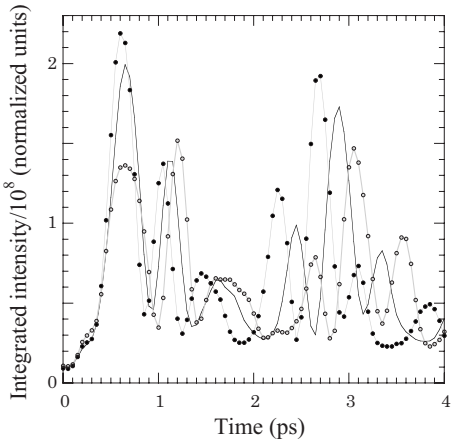

FIG. 5. Time evolution of the integrated x-ray intensities (averaged over 21 independent runs) for the three different sizes of the MD box used for the irradiated system at 300 K: the full line corresponds to the 10 976-atom cell, the full circles to the 8788-atoms cell and the open circles represent the 13 500-atom cell. The signal is clearly size dependent.

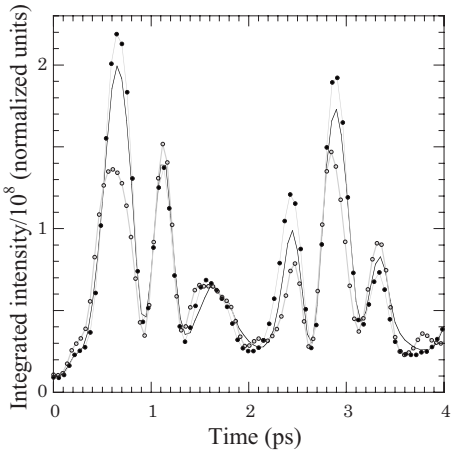

FIG. 6. The same time evolution of the integrated x-ray intensities as displayed in Fig. 5 after the rescaling of the time axis by the linear dimension of the MD box discussed in the text. This rescaling counterbalances the size dependence of the simulation.

proved by the time-rescaled data shown in the insert. When the size of the MD box is increased the height of this peak decreases. Although this time rescaling is numerically identical to the one described above for the phonons, its physical origin is conceptually different. The time rescaling accounts here for the longer time it takes for the cascade to reach the boundary, assuming a constant velocity of propagation. The decrease in the peak when the MD box size is increased indicates that it is an artifact related to the size of the MD box. It is due to a part of the cascade leaving the MD box and re-entering it at the other side due to the PBC.

IV. SUMMARY AND CONCLUSIONS

In summary, we have carried out a MD simulation of displacement cascades in copper. The atomic trajectories have been studied by conventional direct-space analysis, which shows that the number of Frenkel defects is large. In addition, the trajectories have been characterized by calculating their x-ray diffraction patterns as a function of time. These indicate that even at ultrashort times the main effect of the irradiation is an important perturbation of the lattice vibrations.

An important result of our work is that the part of the x-ray intensity that is most representative of the presence of a developing cascade is not the signal from the Frenkel defects but rather that of the perturbed phonons. The contribution to the x-ray intensity from the Frenkel defects is in fact so small with respect to the contribution from the phonons that it can be neglected. The phonon contribution however, can be increased in a real experiment by increasing the cascade density. In our data analysis the cascade density is merely an adjustable parameter. From a given cascade density onward we will start having several cascades developing simultaneously and this will further increase the x-ray intensity. The cascades may even interact, and this is something we could study in the future. All these factors will contribute to an enhanced phonon contribution in the form of thermal diffuse scattering. For inelastic x-ray scattering however, the phonons, whose typical energies lie in the 50 meV regime, cannot be resolved with the x-ray resolution that prevails in a laser experiment (eV regime). This remark also applies in a nonirradiated system but the coherent pile-up of many simultaneous phonons will move the signal out of the elastic resolution window, rendering it observable.[19] Simultaneously, the intensity of the elastic peak will decrease. We can expect this pile-up process also to take place in the irradiated crystal.

In this case, the ideal protocol for probing the ultrashort time physics of displacement cascades should be dynamical rather than static (as in an x-ray diffraction experiment). The relevant analysis tool should then be the dynamical Van Hove correlation function rather than the static correlation function. It may be noted here that rather than inelastic x-ray scattering, we could use inelastic light scattering to probe the cascade. As we have observed in the MD simulations that phonons are strongly altered by a displacement cascade at ultrashort times, measuring the phonons optically might be an interesting experimental approach to *in situ* observation of a displacement cascade.

*marc.hayoun@polytechnique.edu

[1] A. Rousse, P. Audebert, J. P. Geindre, F. Falliès, J. C. Gauthier, A. Mysyrowicz, G. Grillon, and A. Antonetti, Phys. Rev. E **50**, 2200 (1994).
[2] P. Forget, F. Dorchies, J. C. Kieffer, and O. Peyrusse, Chem. Phys. **299**, 259 (2004).
[3] F. Albert, R. Shah, K. Ta Phuoc, F. Burgy, J. P. Rousseau, A. Rousse, A. Pukhov, and S. Kiselev, Int. J. Mod. Phys. B **21**, 497 (2007).
[4] V. Malka, J. Faure, Y. A. Gauduel, E. Lefebvre, A. Rousse, and K. Ta Phuoc, Nat. Phys. **4**, 447 (2008).
[5] M. Borghesi, C. A. Cecchetti, L. Romagnani, P. Antici, P. Audebert, J. Fuchs, E. D'Humières, E. Brambrink, T. Toncian, A. Pipahl, O. Willi, and E. Lefebvre, Int. J. Mod. Phys. B **21**, 590 (2007).
[6] D. J. Bacon, in *Computer Simulation in Materials Science*, edited by H. O. Kirchner, L. P. Kubin, and V. Pontikis (Kluwer Academic, Dordrecht, 1996), p. 189.
[7] D. J. Bacon and T. de-la-Rubia, J. Nucl. Mater. **216**, 275 (1994).
[8] N. V. Doan and F. Rossi, Solid State Phenom. **30-31**, 75 (1992).
[9] A. Barbu and G. Martin, Solid State Phenom. **30-31**, 179 (1992).
[10] E. Balanzat and S. Bouffard, Solid State Phenom. **30-31**, 7 (1992).
[11] M. P. Allen and D. J. Tildesley, *Computer Simulation of Liquids* (Clarendon Press, Oxford, 1987).
[12] G. Ciccotti, D. Frenkel, and I. R. McDonald, *Simulation of Liquids and Solids* (North-Holland, Amsterdam, 1987).
[13] C. Rey-Losada, M. Hayoun, and V. Pontikis, in *Materials Theory and Modelling*, edited by J. Broughton, P. Bristowe, and J. Newsam, MRS Symposia Proceedings No. 291 (Materials Research Society, Pittsburgh, 1993), p. 549.
[14] G. J. Ackland and V. Vitek, in *Atomistic Simulation of Materials: Beyond Pair-Potentials*, edited by V. Vitek and D. J. Srolovitz (Plenum, New York, 1989), p. 193.
[15] V. Rosato, M. Guillopé, and B. Legrand, Philos. Mag. **A59**, 321 (1989).
[16] T. Diaz de la Rubia and M. W. Guinan, Mater. Sci. Forum **97-99**, 23 (1992).
[17] J. M. Ziman, *Principles of the Theory of Solids* (Cambridge University Press, New York, 1972).
[18] D. Waasmaier and A. Kirfel, Acta Crystallogr., Sect. A: Found. Crystallogr. **51**, 416 (1995).
[19] A. M. Lindenberg, I. Kang, S. L. Johnson, T. Missalla, P. A. Heimann, Z. Chang, J. Larsson, P. H. Bucksbaum, H. C. Kapteyn, H. A. Padmore, R. W. Lee, J. S. Wark, and R. W. Falcone, Phys. Rev. Lett. **84**, 111 (2000).